Supporting Information for "The Cluster Virtual Observatory for ULF Waves"

O.D. Constantinescu[1,2], K.H. Fornaçon[1], U. Motschmann[3], I. Richter[1],

K.H. Glassmeier[1]

[1]Institute for Geophysics and Extraterrestrial Physics, TU Braunschweig, Germany

[2]Institute for Space Sciences, Bucharest, Romania

[3]Institute for Theoretical Physics, TU Braunschweig, Germany

Contents of this file

Corresponding author: O. D. Constantinescu, Institute for Geophysics and Extraterrestrial Physics, TU Braunschweig, Germany (d.constantinescu@tu-bs.de)

10. Figure S2: M MFA set
11. Figure S3: B - density set
12. Figure S4: Poynting vector direction set
13. Figure S5: Poynting vector MFA set
14. Figure S6: Yearly configuration plot
15. Figure S7: Monthly configuration plot
16. Figure S8: Daily configuration plot
17. Figure S10: ULF parameters plots CVO web page
18. Figure S11: ULF parameters data CVO web page
19. Figure S12: Tetrahedron configuration plots CVO web page

Introduction

Here we list all the waves and geometric configuration parameters made available through the CVO and we present examples of plots archive and screenshoots of the CVO web interface.

All the parameters are computed in the time frequency domain using (directly or indirectly) a sliding window of 2048 s (34 min and 8 s). The sliding step of 256 s (4 min and 16 s) is one eighth of the window length. For a 24 h interval, 330 evaluations are thus performed on the time axis. A sample rate of one second results in a Nyquist frequency of 0.5 Hz. The frequency resolution from the *Fast Fourier Transform* (FFT) method is equal to the inverse of the window length (1.025 mHz), while the number of frequencies for which each parameter is computed is equal to half of the window size plus one (1025 frequencies). Therefore, for one day interval of data, each parameter is computed for

each cell of a 330×1025 domain in the time-frequency space. To reduce the statistical fluctuations a 5 points boxcar (two points to the left and two points to the right) average over frequency domain is performed for all parameters.

List of ULF parameters available through the CVO

The parameters can be grouped as follows:

- parameters derived from a single physical quantity
  - ⋆ Power spectral densities (PSD)
    - ∘ magnetic field (**B**)
      - ▷ PSD of the coherent part
      - ▷ PSD of distinct components
        - x, y, z in the GSE coordinate system
        - orthogonal and parallel components in the MFA coordinate system
      - ▷ PSD corresponding to distinct polarization modes
        - linear polarized
        - circular polarized
          - · right hand polarized
          - · left hand polarized
    - ∘ electric field (**E**)
      - ▷ total Power spectral density (sum of the PSDs of the three components)
    - ∘ electron density (n)
      - ▷ Power spectral density of the electron density fluctuations
  - ⋆ polarization parameters (**B**)

- coherency between the two principal components
- compression ratio
- ellipticity
- ratio between the intermediate and minimum eigenvalues
- polarization degree

⋆ directions obtained from magnetic field variance analysis ($\mathbf{B}$)

- angle between the wave vector and the mean magnetic field direction
- angle between the wave vector and the poloidal direction in SM coordinates
- angle between the wave vector and the radial direction in SM coordinates
- angle between the wave vector and the toroidal direction in SM coordinates
- azimuth angle of the wave vector in GSE coordinate system
- elevation angle of the wave vector in GSE coordinate system
- azimuth angle of the maximum variance direction in GSE
- elevation angle of the maximum variance direction in GSE

• parameters derived from more physical quantities

⋆ magnetic field - electron density (B, n)

- coherency between the magnetic field and density variations
- phase shift between the magnetic field module and density variations
- co-spectrum between the magnetic field module and density variations
- quad-spectrum between the magnetic field module and density variations

⋆ magnetic field - electric field ($\mathbf{B}, \mathbf{E}$)

- Poynting vector module (S)

- components of the Poynting vector ($\mathbf{S}$)
  - x, y, z in GSE coordinate system
  - parallel and orthogonal components on the mean $\mathbf{B}$
- direction of the Poynting vector
  - angle between the Poynting vector and the wave vector
  - angle between the Poynting vector and the mean magnetic field
  - angle between the Poynting vector and the poloidal direction in SM
  - angle between the Poynting vector and the radial direction in SM
  - angle between the Poynting vector and the toroidal direction in SM
  - azimuth angle of the Poynting vector in GSE
  - elevation angle of the Poynting vector in GSE

Description of the wave vector direction set

The first and the last two panels in this set illustrated in Fig. S1 are the same with the corresponding ones in the *Basic parameters* set. The total PSD is replaced in the second panel by the PSD of the coherent part of the fluctuations computed from the coherent intensity Eq. (14): $P_{\rm coh} = 2WI_{\rm coh}$.

The two panels in the third row show the direction of the wave vector as scatter plots in the (θ, φ) domain. The time is colour coded. The directions corresponding to 30° cones around the positive and negative directions of the coordinate system axes are plotted as ellipses for the x and y axes and as horizontal lines for the z axis. The coordinate system used for the left hand side panel is a Local Magnetic Coordinate (LMC) system defined starting from the position vector of the spacecraft in the Solar Magnetic (SM) coordinate system (Laundal & Richmond, 2017): The z axis is defined as the geocentric

radial direction, the y axis is defined by the cross product of the z axis of the SM coordinate system and the radial direction: $\hat{\boldsymbol{e}}'_y = \hat{\boldsymbol{e}}^{\rm SM}_z \times \hat{\boldsymbol{e}}'_z / |\hat{\boldsymbol{e}}^{\rm SM}_z \times \hat{\boldsymbol{e}}'_z|$. This axis points eastward in the toroidal direction. The x axis completes the right handed system and points southward in the poloidal direction: $\hat{\boldsymbol{e}}'_x = \hat{\boldsymbol{e}}'_y \times \hat{\boldsymbol{e}}'_z$. The LMC system is useful in the inner magnetosphere where the dipole field dominates. The right hand side panel uses the GSE coordinate system with the x axis pointed towards the Sun and the y axis in the ecliptic plane. In accord with the conclusions drawn from the previous plot set, the propagation direction is not well defined in front of the bowshock (black and cyan colours). Inside the bowshock it seems that the waves prefer to propagate in the poloidal-toroidal plane, avoiding radial propagation. Together with the position in the dayside magnetosheath, this suggests that in this case the waves propagate more along the magnetosheath than in the cross-magnetosheath direction. Considering the (anti)parallel to the magnetic field propagation found previously, this reflects the draping of the magnetic field lines around the magnetopause.

The parallel propagation can also be observed in the next two panels which are similar with the panels showing the wave vector direction in the previous plot set. The difference is the coordinate system which now is the LMC system. The θ angle made with the radial direction shows a preference towards 90°. The φ angle made with the poloidal-toroidal plane is reduced to angles corresponding to inward propagation ($\theta \geq 90°$).

Description of the B MFA set

Mean Field Aligned (MFA) related parameters are shown in Fig. S2. The top panel is similar with the top panels from the previous discussed plot sets but now the magnetic field time series are represented in the MFA coordinate system. This system has the z axis

aligned with the mean magnetic field vector. The mean magnetic field vector is computed using a boxcar average with the width equal to the sliding step $W/8 = 256\,\mathrm{s}$ used to compute the PSD. The y axis is orthogonal to the mean magnetic field - position vector plane: $\hat{\boldsymbol{e}}_y^{\mathrm{MFA}} = \hat{\boldsymbol{e}}_r^{\mathrm{GSE}} \times \hat{\boldsymbol{e}}_z^{\mathrm{MFA}} / |\hat{\boldsymbol{e}}_r^{\mathrm{GSE}} \times \hat{\boldsymbol{e}}_z^{\mathrm{MFA}}|$ and in the inner magnetosphere points roughly in the westward azimuthal direction. The x axis completes the right-handed system: $\hat{\boldsymbol{e}}_x^{\mathrm{MFA}} = \hat{\boldsymbol{e}}_y^{\mathrm{MFA}} \times \hat{\boldsymbol{e}}_z^{\mathrm{MFA}}$, roughly radial in the inner magnetosphere. The x and y directions can substantially deviate from the azimuthal and radial directions in the vicinity of the cusp regions and outside the dipolar field and they take more or less arbitrary directions outside the magnetosphere and in disturbed regions.

The three panels below the time series panel show the power spectral densities for the three components of the magnetic field in the MFA system. In our case, x and y (radial and azimuthal) directions concentrate most of the wave energy, while little energy is contained in the fluctuations parallel to the mean magnetic field. This is made more obvious by the next panel which illustrates the compression ratio C Eq. (18). Most of the magnetic field fluctuations are clearly perpendicular, with the exception of some low frequency fluctuations close to the bowshock crossings and of the waves around 04 UT.

Though the parameters shown in the last three panels are not directly related to the MFA coordinate system, we coose to include them in this set. The wave normal angle and ellipticity were discussed above. The coherence Eq. (13) is equivalent with the polarization degree Eq. (4) only when the noise contribution is isotropic. See e.g. Jones (1979).

Description of the B – density set

This set, illustrated in Fig. S3, shows the parameters related to the electron density fluctuations. Because of time resolution and data availability restrictions of the particle

instruments we derive the electron density from the spacecraft potential using the relations provided by Lybekk et al. (2012). The exact parameters used to derive the electron density were only determined up to 2010. From 2010 on we use the 2010 parameters. This means that the estimated electron density can deviate from the real one. However, the most important density related parameters, the coherence and the phase difference between the magnetic field and density fluctuations are independent on eventual offset or scaling errors in the density. Therefore these parameters are also reliable after 2010. The co- and quad-spectrum values are affected by these errors, but they still describe qualitatively the relation between the magnetic field and the density.

The black line in the top panel shows the magnetic field magnitude smoothed using a sliding window of 1024 s. The red line shows the density. The total PSD of the magnetic field in the next panel is the same as the one in Fig. 1 with the addition of the electron density over-plotted with the yellow line using logarithmic scale. The power spectral density of the density fluctuations computed using the same procedure as for the PSD of the magnetic field is shown in the next panel.

The coherency between the magnetic field fluctuations and the density fluctuations , γ_{Bn} computed from Eq. (13) is plotted in the next panel, with values below 0.6 masked out. The power and polarization masks are applied as well. The coherency is mostly low inside the magnetosheath , but somewhat larger in front of the magnetosheath. Even for these relatively low values, there is still coherent interaction between the field and the particles as reflected by the magnetic field - density phase differences plotted in the panel below. The colours are assigned to the phase difference $\Delta\varphi_{Bn} = \varphi_B - \varphi_n$ as follows: red for opposite phase $(-180,^\circ -135^\circ)$ and $(135^\circ, 180^\circ)$, blue for in phase oscillations $(-45^\circ, 45^\circ)$, yellow for

retarded magnetic field oscillations $(45°, 135°)$, and green for retarded density oscillations $(-135°, -45°)$. In addition to the power and polarization masks, a mask for coherency $\gamma_{Bn} < 0.5$ was applied. The larger coherency in front of the magnetosheath is reflected in much more stable phase differences across the time-frequency domain as inside the magnetosheath. Here, the field oscillate in opposition to the density, indicating consistent coupling between field and particles. Inside the high polarization time-frequency domains in the magnetosheath, the density fluctuations seem to be retarded from the magnetic field fluctuations, suggesting that the magnetic field drives the density and not the other way around.

The last three panels in this set are the same as those in the *basic parameters* set in Fig. 1.

Description of the Poynting vector direction set

This set, illustrated in Fig. S4, aims to show the direction in which the waves energy flows. The magnetic field time series in the first panel is the same as in Fig. 1. The next panel shows the module of the Poynting vector Eq. (22), with no mask applied. The electric field measured by the Electric Field and Wave Experiment (EFW) (Gustafsson et al., 1997) is downloaded from the CSA at a resolution of 25 vectors per second when available, otherwise a much lower resolution of one vector each 4 s is used. One should consider the caveats of the electric field instrument before interpreting these plots. For instance since the end of 2001 only three probes are functional on Cluster 1, same applies to Cluster 3 after mid 2002, and to Cluster 2 after mid 2007. The $\boldsymbol{v} \times \boldsymbol{B}$ electric field is removed and no field-aligned electric field is allowed.

The four panels below, showing the direction of the Poynting vector, are similar and use the same coordinate system as for the wave vector direction in Fig. S1. However, in contrast with the wave vector direction, no sign uncertainty exists, and the Poynting vector direction is much more confined indicating a clear anti-sunward flow of the energy in the GSE (θ, φ) right hand side plot and a westward toroidal flow in the left hand side plot. Remarkably, the energy flows in this direction during the entire day, despite increasing distance to the equatorial plane. Data points with the Poynting vector module below $0.5\,\mu\mathrm{W\,km^{-2}\,Hz^{-1}}$ were discarded, and power and polarization masks were applied.

The penultimate panel shows the angle between the Poynting vector and the mean magnetic field in the time-frequency domain. Unlike the wave normal angle plotted in Fig. S1, which for the polarized waves inside the magnetosheath keeps a constant (anti)parallel direction to the magnetic field, the Poynting vector changes from anti-parallel near the bowshock to parallel towards the end of the interval reaching in the process large angles to the magnetic field.

Description of the Poynting vector MFA set

The first two panels of this last set of plots shown in Fig. S5, are the same as the first two panels in Fig. S1, and the last panel is the same as the Poynting vector - mean magnetic field angle panel in Fig. S4. The remaining panels show the total power spectral density of the electric field, the components of the Poynting vector in the mean field aligned system defined for the *B MFA* plot set, and the angle between the wave vector and the Poynting vector, reduced to $(0°, 90°)$ due to the sign uncertainty.

Description of the yearly, monthly and daily configuration plots

Yearly overview plots for the entire mission duration are provided, an example being shown in Fig. S6. These are similar with the four years plots but are separated on months and in addition the trajectories in the (e,p) domain are also plotted inside the right hand side colour keys.

A more detailed view of the tetrahedron geometry is offered by the monthly plots. The plot for January 2005 is shown in Fig. S7. The projections of the orbit of the formation barycentre on the three GSE planes allow for a quick estimation of the tetrahedron shape for different magnetospheric regions, while the size of the tetrahedron together with the corresponding colour encoded shape is shown in the fourth panel. To aid linking of the line colour with the (e,p) space and to give a better overview of which regions of the (e,p) space are being visited during the month, the trajectory in the shape space is plotted with white in the colour-key.

The most detailed view of the geometric parameters is given by the daily plots. Fig. S8 is an example for 1st of January 2005. To give an overview of the magnetic field measurements the top panel shows the magnetic field magnitudes measured by the four spacecraft (C1 - black, C2 - red, C3 - green, C4 - blue). The magnetospheric regions in which each spacecraft finds itself are represented by the coloured bars at the bottom of the panel. Top bar for C1, bottom bar for C4. The magnetospheric regions are determined from the Goddard SSCWeb interface `http://sscweb.gsfc.nasa.gov` using IGRF internal and Tsyganenko 89C external model. The six inter-spacecraft distances are presented in the next panel, followed by the geocentric distances for all spacecraft an for the barycentre of the formation. The fourth panel shows the degeneration degree, defined as the radial coordinate in the (e, p) domain: $0 \leq \sqrt{e^2 + p^2} \leq \sqrt{2}$. A small degeneration indicates a

near regular tetrahedron. The degeneration increases as the tetrahedron departs from the regular shape. The bottom left plot shows the trajectory in the (e,p) domain with the time colour coded. The projections of the orbit on the GSE (x,y), (x,z), and (y,z) planes and the geocentric distance of the barycentre are shown in the four bottom right plots.

References

Gustafsson, G., Bostrom, R., Holback, B., Holmgren, G., Lundgren, A., Stasiewicz, K., ... Wygant, J. (1997, January). The Electric Field and Wave Experiment for the Cluster Mission. *Space Science Reviews*, *79*, 137-156.

Jones, A. (1979). On the Difference Between Polarisation and Coherence. *Journal of Geophysics*, *45*, 223-229.

Laundal, K. M., & Richmond, A. D. (2017, March). Magnetic Coordinate Systems. *Space Sci. Rev.*, *206*(1-4), 27-59. doi: 10.1007/s11214-016-0275-y

Lybekk, B., Pedersen, A., Haaland, S., Svenes, K., Fazakerley, A. N., Masson, A., ... Trotignon, J.-G. (2012, January). Solar cycle variations of the Cluster spacecraft potential and its use for electron density estimations. *Journal of Geophysical Research (Space Physics)*, *117*, A01217. doi: 10.1029/2011JA016969

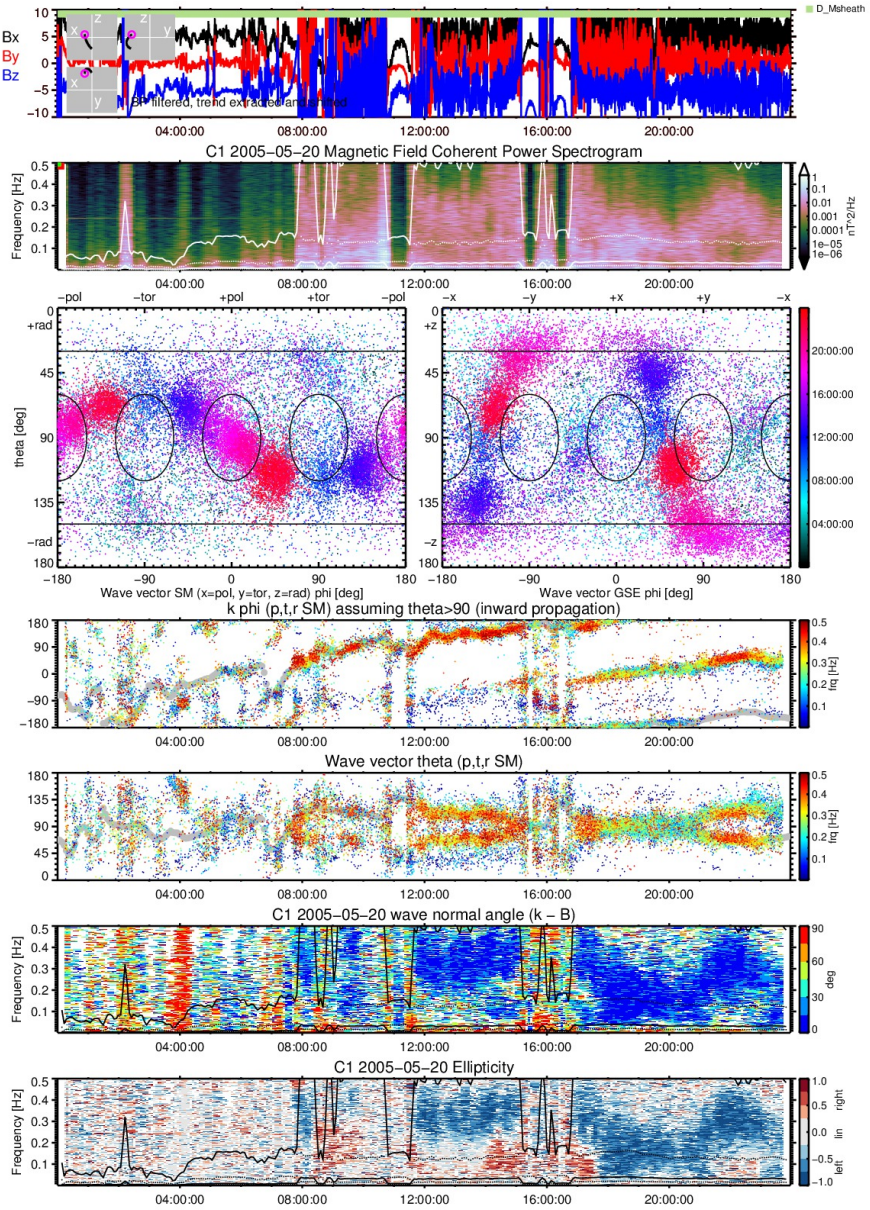

Figure S1. The *wave vector direction* plot set for C1 on 20th May 2005. The top and bottom two panels are the same as in Fig. 1. The second panel shows the PSD of the coherent part of the magnetic field. The third raw shows the wave vector orientation in the LMC system (left) and in GSE (right). The two panels below show the wave vector orientation in the LMC system. The mean magnetic field is plotted with the thick grey line.

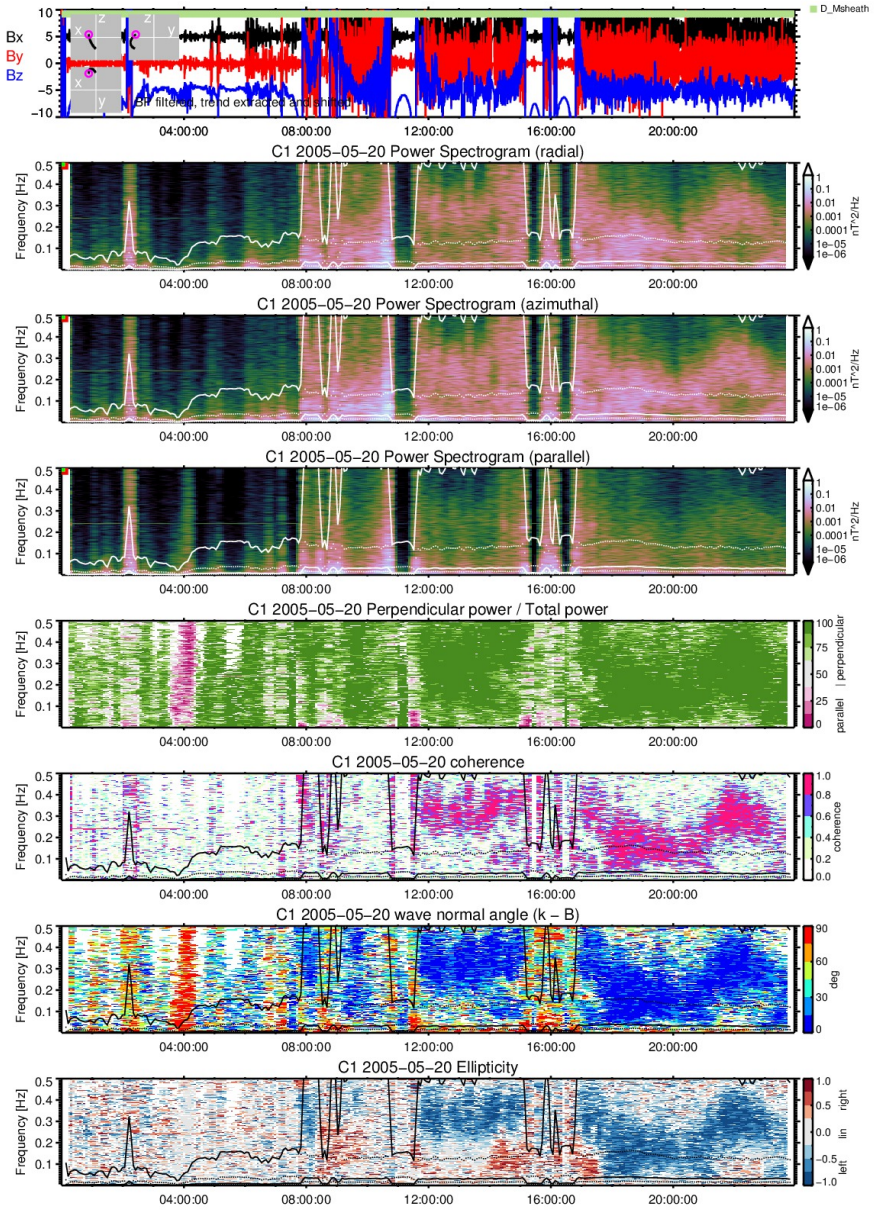

Figure S2. The *B MFA* plot set for C1 on 20th May 2005. The top panel is similar with the top panel in Fig. 1. The three panels below show the PSD of the magnetic field in the MFA system. The next two panels show the compression ratio and the coherency. The last two panels are the same as in Fig. 1.

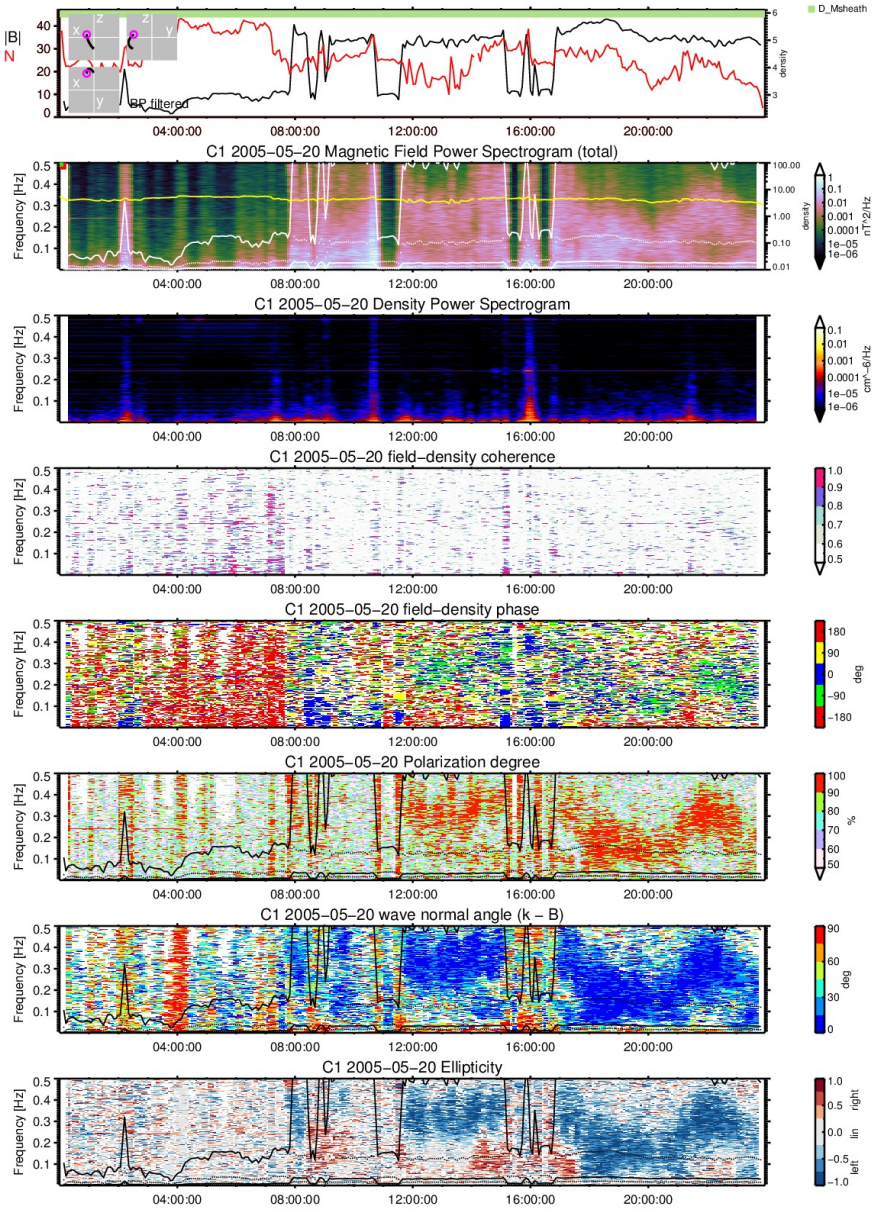

Figure S3. The *B* - *density* plot set for C1 on 20th May 2005. The top panel shows the module of the magnetic field (black) and the plasma density (red), both smoothed with a 512 s window; The second panel is the same as the second panel in Fig. 1 with the addition of the plasma density shown by the yellow line; The third panel shows the PSD of the density fluctuations; The fourth panel shows the coherency between the magnetic field and the plasma density fluctuations; The fifth panel shows the phase difference between the magnetic field and the density fluctuations. The bottom three panels are the same as in Fig. 1.

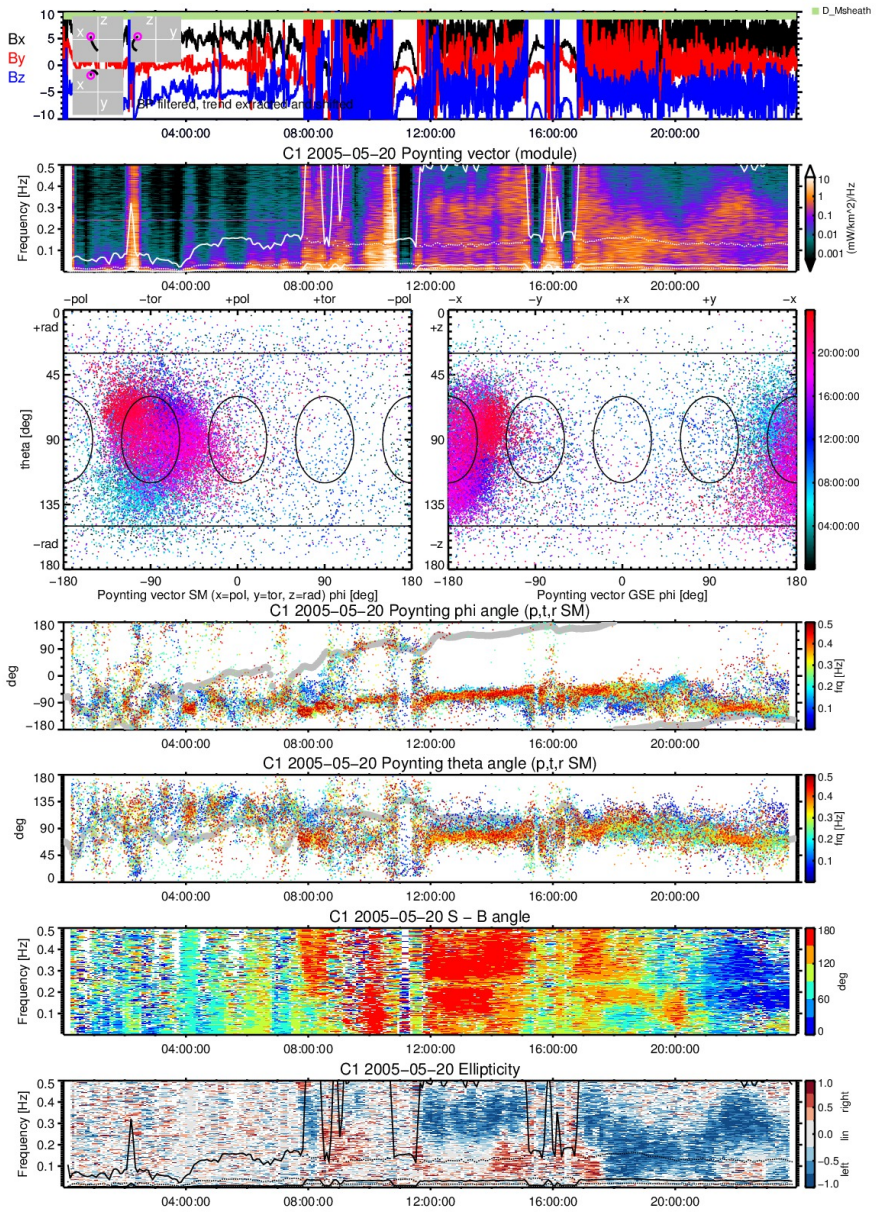

Figure S4. The *Poynting vector direction* plot set for C1 on 20th May 2005. The top and bottom panels are same as in Fig. 1. The second panel shows the PSD of the Poynting vector module and the gyrofrequencies of H, He, and O. The two panels in the third raw are similar with those in Fig. S1 but instead of the wave vector direction show the Poynting vector direction. The next two panels show the Poynting vector direction in the LMC system. The second panel from bottom shows the angle between the Poynting vector and the mean magnetic field.

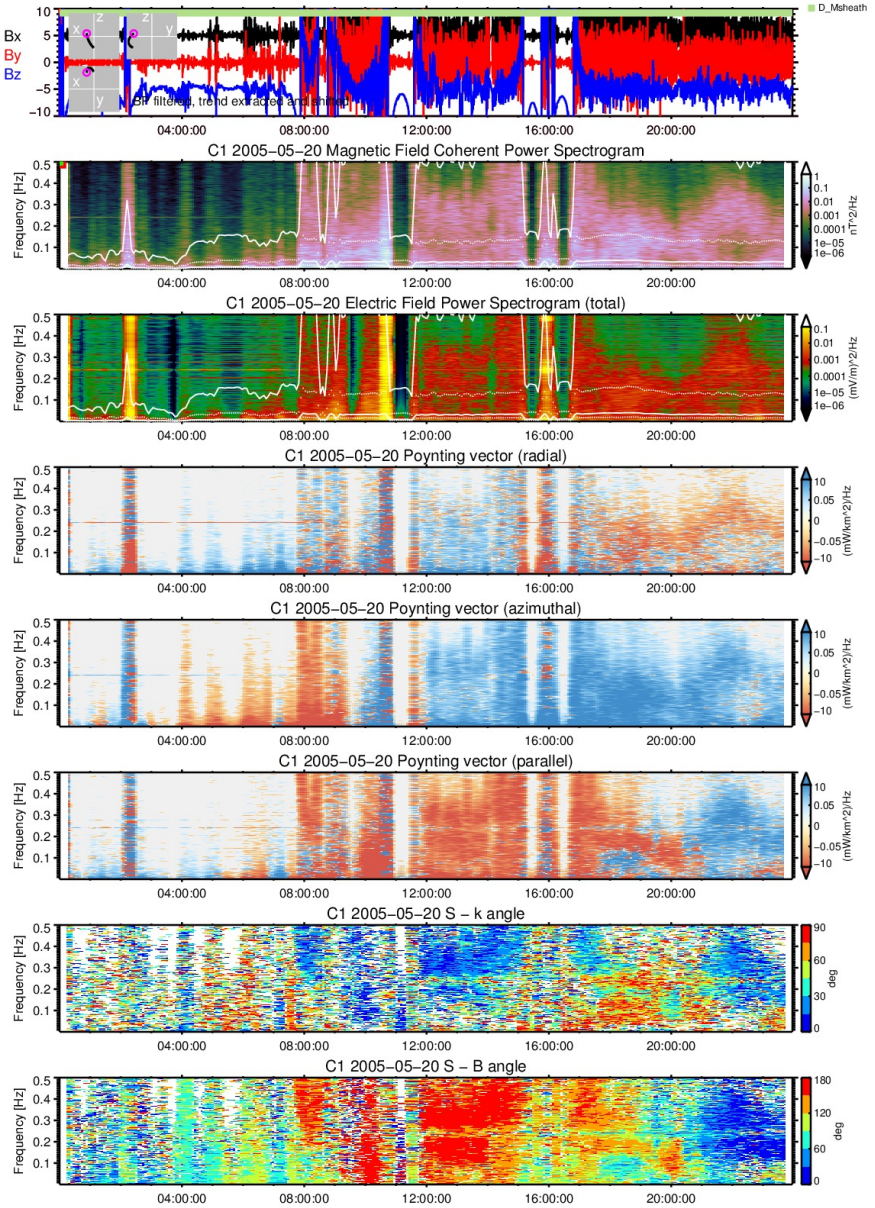

Figure S5. The *Poynting vector MFA* plot set for C1 on 20th May 2005. From top to bottom: Magnetic field in MFA system; PSD of the coherent part of magnetic field fluctuations; Sum of the PSD of the electric field components; Radial, azimuthal, and parallel components of the Poynting vector in the MFA system; The angle between the Poynting vector and the wave vector; The angle between the Poynting vector and the mean magnetic field.

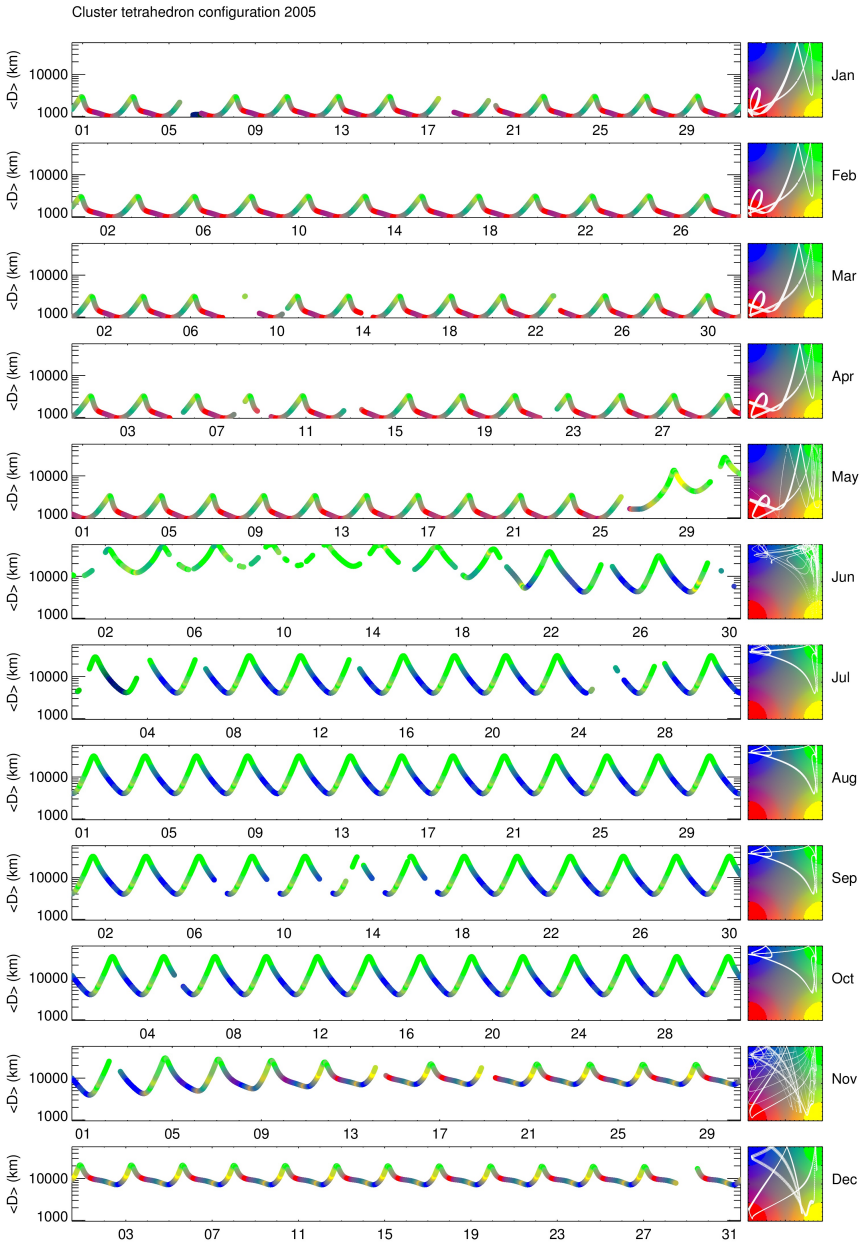

Figure S6. Yearly overview of the mean separation and tetrahedron shape for 2005. The tetrahedron shape is colour encoded and the trajectories in the (e,p) domain are plotted with white in the colour-keys for each month.

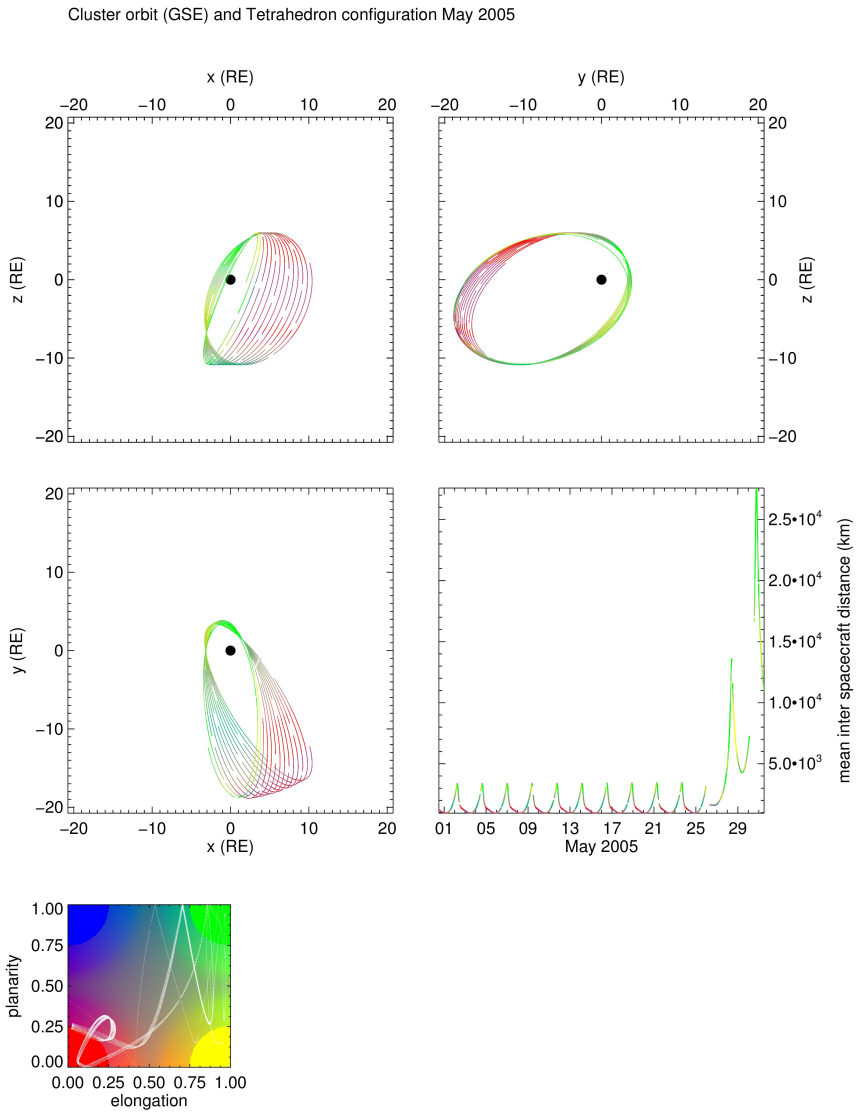

Figure S7. Orbit and geometric parameters of the Cluster tetrahedron during May 2005. The orbits of the formation barycentre are plotted in GSE coordinates and colour codded for the shape with the colour-key in the lower left. The trajectory in the (e,p) plane is shown with white in the colour-key.

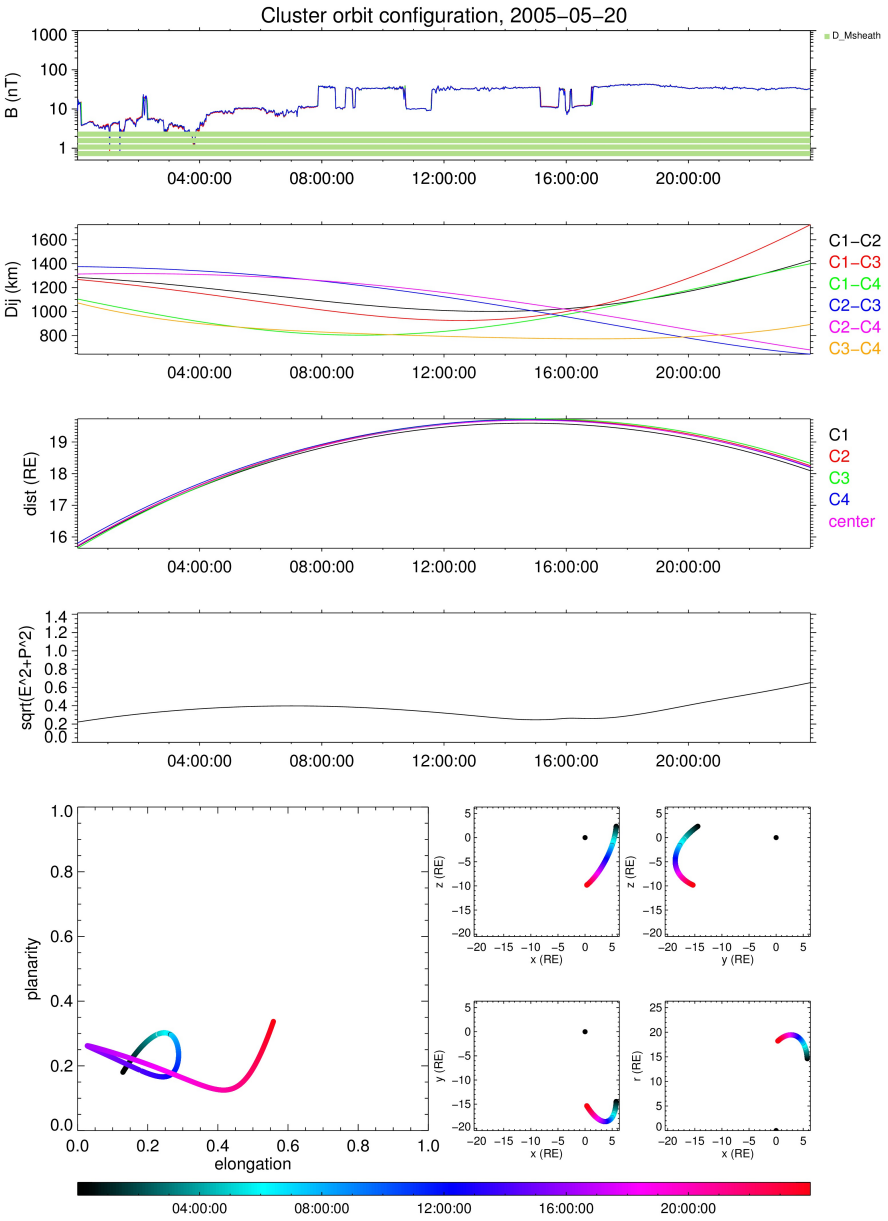

Figure S8. Daily plot for 20th May 2005. From top to bottom: Magnetic field module for the four spacecraft and the magnetospheric regions from SSCWeb. Inter-spacecraft distances. Radial distances for the spacecraft and for the formation barycentre. Degeneration degree of the tetrahedron. Bottom left plot: trajectory in the (e,p) domain, colour encodes the time. Bottom right four plots: barycentre orbit in GSE and barycentre radial distance.

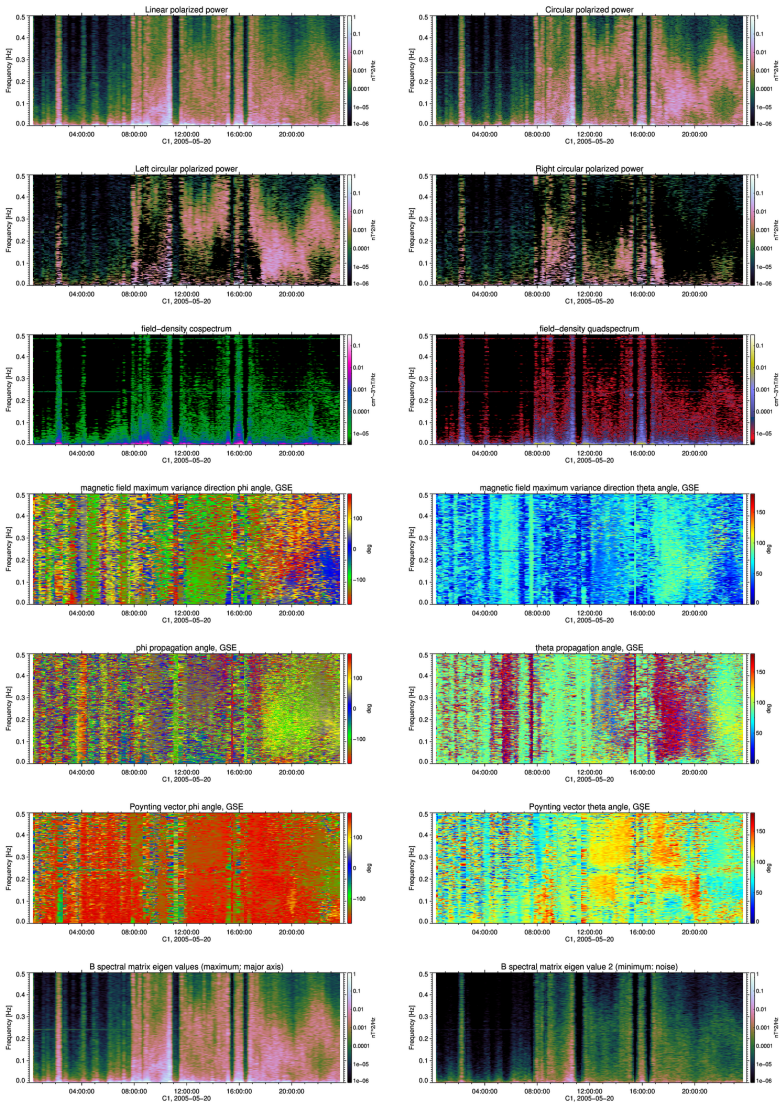

Figure S9. Subset of low resolution quick-view plots for the HDF data archive. No masks are applied. The first panel shows the power spectral density of the linear polarized part of the waves, $P_{\rm lin} = 2A_{\rm lin}^2$, with the amplitude of the linear part, $A_{\rm lin}$ from Eq. (16). The PSD of the circular polarized part of the waves is shown next. The circular polarized waves are further divided into the left $P_{\rm left} = 2(A_{\rm left}^2 - A_{\rm right}^2)|_{>0}$ and the right $P_{\rm right} = 2(A_{\rm right}^2 - A_{\rm left}^2)|_{>0}$ polarization in the following two panels. The co- and quad-spectrum of the magnetic field - density fluctuations are shown in the next row. The following three rows show the directions of the magnetic field maximum variance, wave propagation direction, and Poynting vector in GSE coordinates. The last two panels show the maximum and the minimum eigenvalues of the magnetic field spectral matrix.

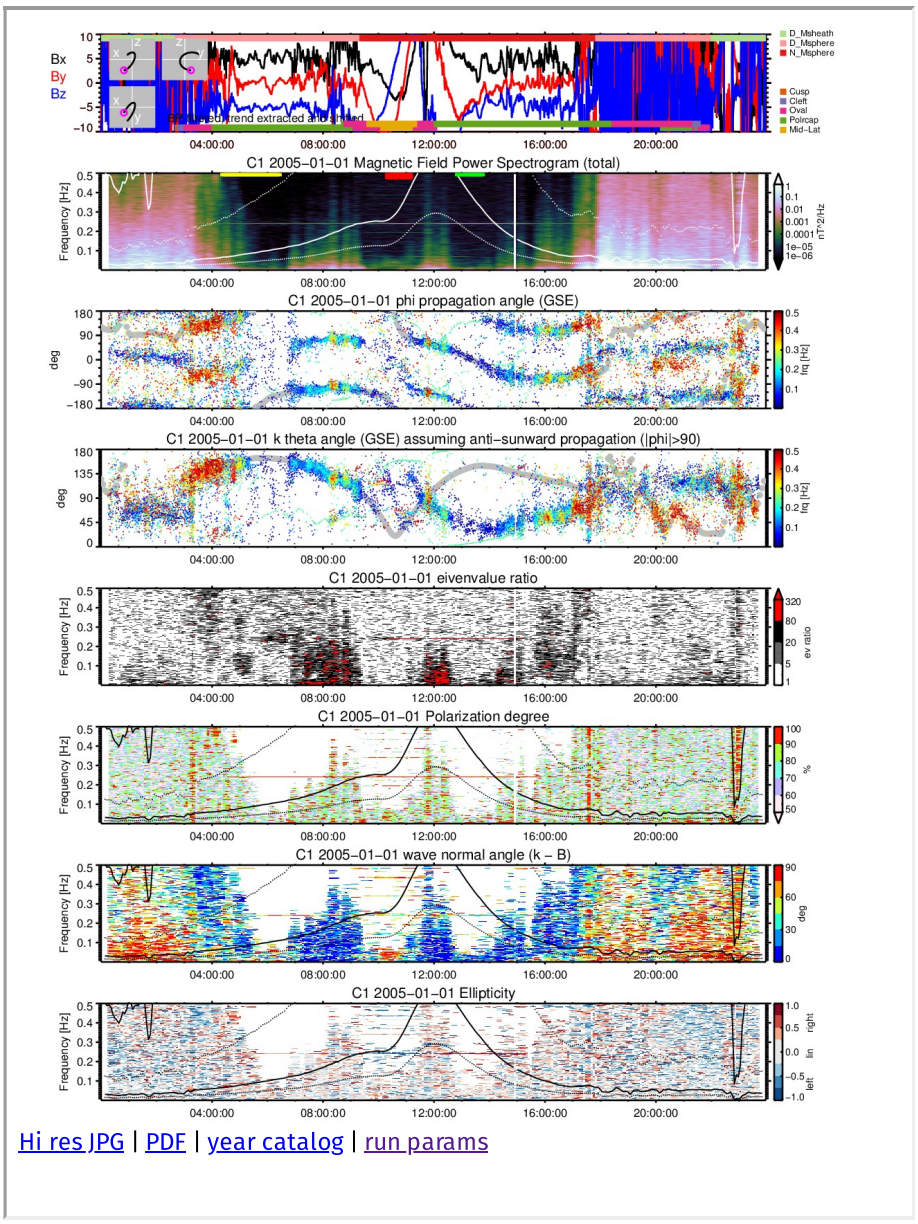

Figure S10. The plots section of the CVO.

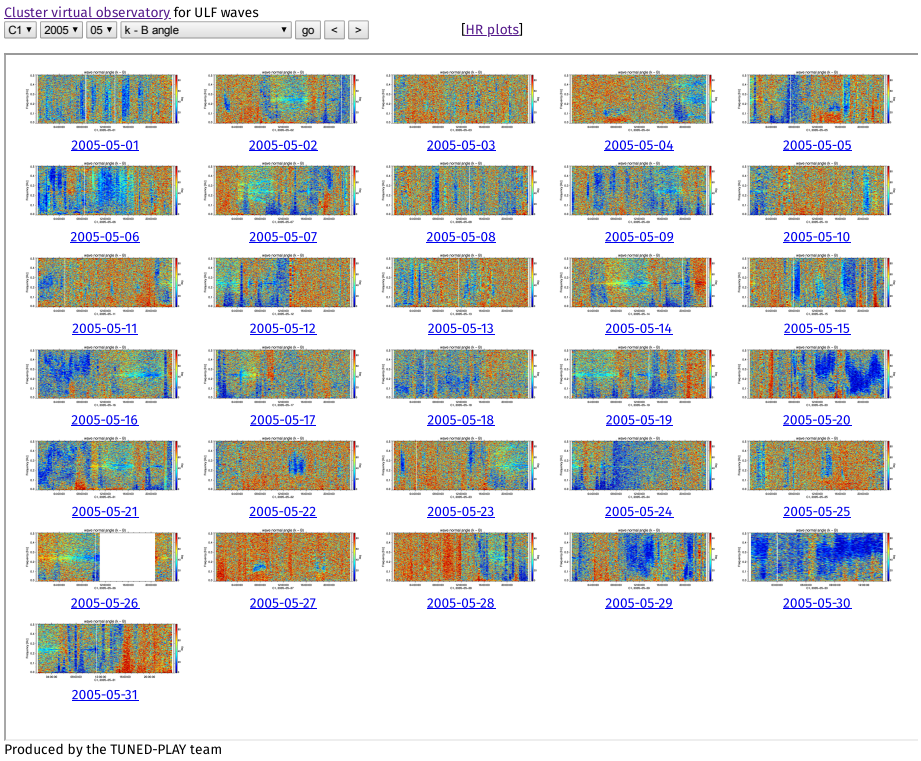

Figure S11. The data section of the CVO.

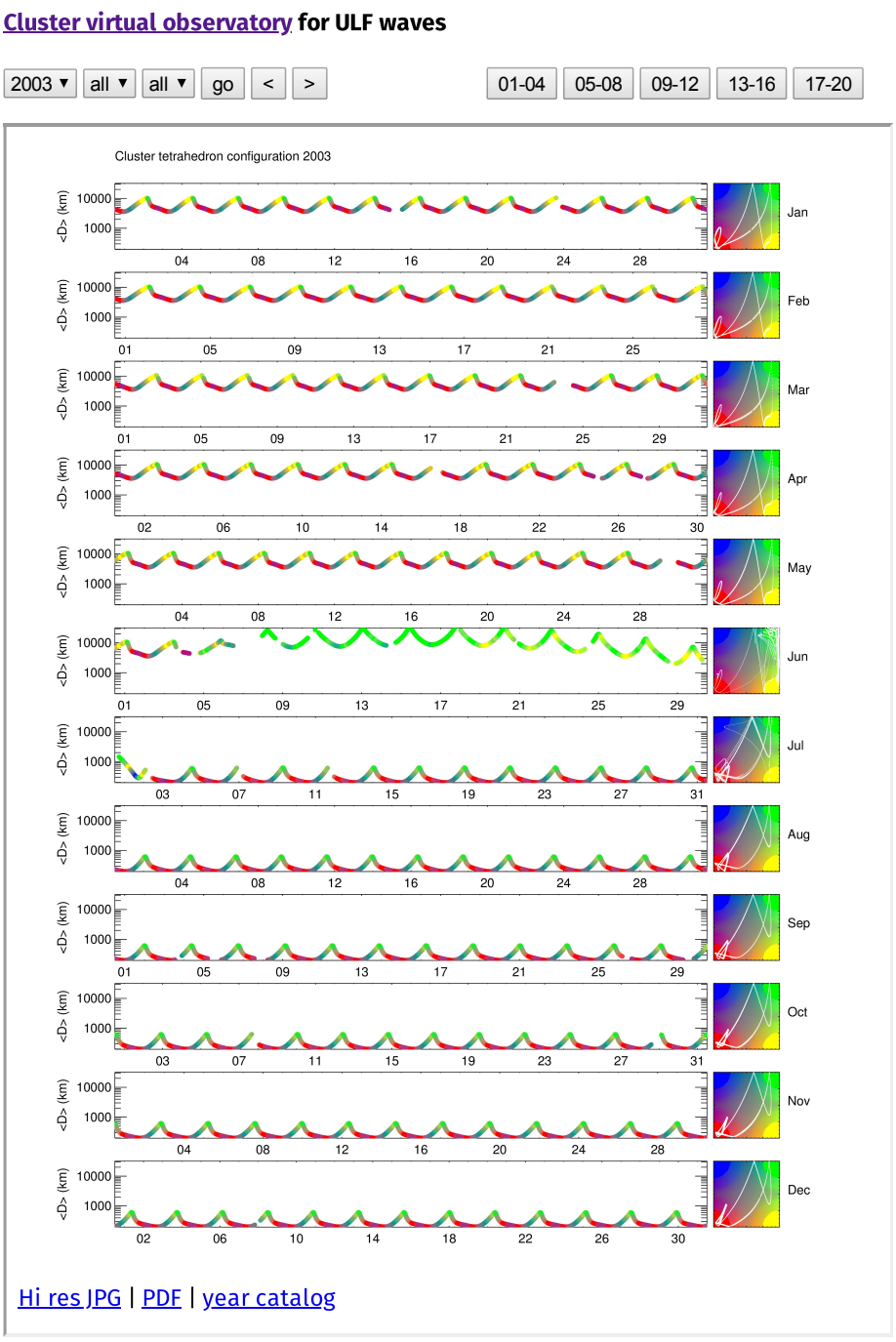

Figure S12. The tetrahedron geometry section of the CVO.